ACS APPLIED MATERIALS & INTERFACES

Research Article

www.acsami.org

Design of a High Performance Thin All-Solid-State Supercapacitor Mimicking the Active Interface of Its Liquid-State Counterpart

Bihag Anothumakkool,[†] Arun Torris A. T.,[‡] Siddheshwar N. Bhange,[†] Sreekuttan M. Unni,[†] Manohar V. Badiger,[‡] and Sreekumar Kurungot*[,†]

[†]Physical and Materials Chemistry Division and [‡]Polymer Science and Engineering Division, CSIR-National Chemical Laboratory, Pune 411008, Maharashtra, India

Supporting Information

ABSTRACT: Here we report an all-solid-state supercapacitor (ASSP) which closely mimics the electrode−electrolyte interface of its liquid-state counterpart by impregnating polyaniline (PANI)-coated carbon paper with polyvinyl alcohol-H_2SO_4 (PVA-H_2SO_4) gel/plasticized polymer electrolyte. The well penetrated PVA-H_2SO_4 network along the porous carbon matrix essentially enhanced the electrode−electrolyte interface of the resulting device with a very low equivalent series resistance (ESR) of 1 Ω/cm^2 and established an interfacial structure very similar to a liquid electrolyte. The designed interface of the device was confirmed by cross-sectional elemental mapping and scanning electron microscopy (SEM) images. The PANI in the device displayed a specific capacitance of 647 F/g with an areal capacitance of 1 F/cm^2 at 0.5 A/g and a capacitance retention of 62% at 20 A/g. The above values are the highest among those reported for any solid-state-supercapacitor. The whole device, including the electrolyte, shows a capacitance of 12 F/g with a significantly low leakage current of 16 μA^2. Apart from this, the device showed excellent stability for 10000 cycles with a coulombic efficiency of 100%. Energy density of the PANI in the device is 14.3 Wh/kg.

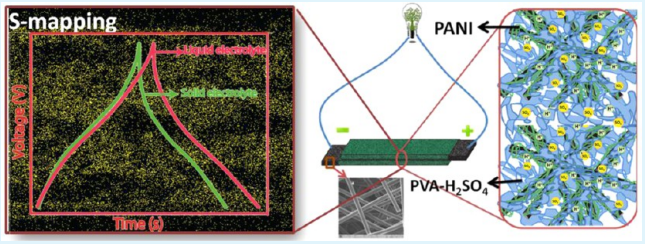

KEYWORDS: *supercapacitor, polyaniline, polyvinyl alcohol, all-solid-state, cyclic voltametry, impedance analysis*

1. INTRODUCTION

Design and development of efficient energy storage systems has become increasingly important for effectively utilizing the interrupted/or intermittent power outputs from natural renewable energy resources.[1] Among the various energy storage devices, electrochemical energy storage systems, such as batteries[2,3] and supercapacitors[4−9] are highly efficient and environmentally benign. Electrochemical supercapacitors or ultracapacitors are very promising over batteries in terms of their high power density.[6,10] Fast charge−discharge rate, high coulombic efficiency, long cycle life, and environmental benign nature are the major advantages of supercapacitors over lithium ion batteries which make them ideal candidates for energy storage. However, liquid electrolytes in conventional electrochemical energy storage devices raise safety issues and thus require high-standard safety encapsulation materials and technologies.[10] Replacement of liquid electrolyte in the energy storage devices with a solid counterpart is thus very promising for developing thin, lightweight, economically viable and flexible future devices.

Polymer electrolytes[11−16] have been extensively studied as electrolytes in supercapacitors and lithium batteries. Among the various polymer electrolytes, gel/plasticized electrolytes[12,13] shows ambient conductivity and desirable mechanical properties and are promising electrolyte materials to replace conventional liquid electrolyte in supercapacitors. Many of the earlier studies utilized gel electrolyte as a film[14,15,17−19] between the electrodes, which resulted in low electrode−electrolyte interfacial area with poor charge storage properties. Apart from the low charge storage properties, total device resistance increases because of high contact resistance arising from the low integrity of the electrode−electrolyte material.[19−21] Very low equivalent series resistance (ESR) is highly desirable for the storage device as the power rate of the device is determined by the relation $P_{max} = V^2/4R$. In recent studies, researchers have been successful in developing free-standing electrode materials for fabricating flexible solid-state devices.[20,22] Here also, these polymer electrolyte films are not intercalated with electrode material which in turn decreases the electrode−electrolyte interfacial area, leading to low capacitance and high ESR. To find a promising solid counterpart for replacing liquid electrolytes in supercapacitors we need an electrode−electrolyte interface in the solid-state system which mimics the liquid−solid interface in the conventional systems.

Here, we could closely mimic the electrode−electrolyte interface obtainable from a liquid electrolyte for the solid-state-supercapacitors, by utilizing the high porosity of conducting carbon paper and tunable viscosity characteristics of the gel electrolyte. Carbon paper used for this purpose possesses very low sheet resistance (0.26 Ω/square), low density (0.4 g/cm^3),

Received: October 2, 2013
Accepted: December 6, 2013
Published: December 6, 2013

and high porosity (97%), which makes it a versatile candidate for fabricating the supercapacitor electrodes. This type of carbon paper also plays a crucial role in membrane electrode assemblies of polymer electrolyte membrane fuel cells because of its advantages mentioned above.[23] The polymer electrolyte selected here is a polyvinyl alcohol (PVA)-H_2SO_4 gel/plasticizer, which is known for its high conductivity and flexibility.[24] Because of the high porosity of the carbon substrate, PVA-H_2SO_4 is successfully intercalated even after the loading of the electrode material. This was further assisted by the presence of water, which played a critical role in reducing the density of PVA to enable its easy penetration into the micropores of the carbon paper. Apart from acting as an enhanced interface, porous carbon backbone gives an adequate electrical contact within the network, which helps in maintaining very low ESR. Meantime, the surface layer of the gel electrolyte eventually functions as a separator between the electrodes when the two electrodes are combined to form a single cell unit. Polymer electrolyte intercalated inside the carbon fiber matrix also helps in improving the mechanical strength of the carbon paper, as it can induce flexibility because of the presence of PVA and reduce its brittleness. The selected electrode material is polyaniline (PANI),[25] which is known for its very high theoretical capacitance (2000 F/g)[26,27] even though bulk PANI shows a significantly low value of 300 F/g or lower because of its poor conductivity and low surface area.[28,29] Here, usage of porous carbon fiber paper helps in improving the specific capacitance of PANI by increasing its electrode−electrolyte interfacial area and conductivity in liquid as well as solid electrolytes.

2. EXPERIMENTAL SECTION

Materials. Aniline, ammoniumpersulfate $(NH_4)_2S_2O_8$, polyvinylalcohol (PVA), and N-methylpyrrolidone (NMP) were purchased from Aldrich Chemicals. Polyvinyl alcohol (PVA) (M.W 1,15,000; 98−99 mol % hydrolyzed) was supplied by Loba Chemie. Sulfuric acid (H_2SO_4) and hydrochloric acid (HCl) were procured from Rankem Chemicals. All the chemicals were used as received without any further purification. A polytetrafluoroethylene (PTFE) filter paper (pore size, 0.45 μm; Rankem) was used for the filtration. Carbon paper having a thickness of 0.3 mm was purchased from Toray Japan. Polypropylene membrane of 25 μm from Celgard was used as a separator when liquid was used as the electrolyte.

Synthesis of PANI: PANI was prepared by adopting a reported method.[25] In a typical synthesis, to an ice cold solution of 1 mL of aniline in 50 mL of 1 M HCl, precooled solution of $(NH_4)_2S_2O_8$ in 50 mL of 1 M HCl was added dropwise and stirred for 6 h. The green colored PANI solution was filtered and washed with DI water and dried at 60 °C.

Preparation of PVA-H_2SO_4 Solutions and Film. Approximately 2 g of PVA was weighed and transferred onto a 100 mL RB flask containing 20 mL of deionized water to prepare a 10 wt % PVA solution. The mixture was heated at 85 °C with constant stirring until a clear solution of PVA was obtained. This was subsequently cooled to room temperature. Approximately, 2 g of concentrated H_2SO_4 was added to the solution and stirred gently for 30 min to obtain 1:1 PVA-H_2SO_4 solution. Films were prepared by pouring 7 g of PVA-H_2SO_4 solution into a glass Petri-dish having 7 cm diameter and was kept in an oven initially at 60 °C for 2 h and later at 40 °C for 6 h to obtain a uniform transparent PVA-H_2SO_4 film.

Electrode Preparation and Device Fabrication. Electrodes were prepared as follows: A paste of PANI was made with NMP and this was coated onto 1 cm^2 area of a Toray carbon paper (non teflonated) having a total dimension of 1 × 2 cm^2 using a K-control coater. The excess dimension outside the PANI coated area was kept to utilize it as the current collector during the measurements. PANI to NMP ratio was fine-tuned to get a uniform deposition of PANI inside the carbon matrix. Different loading of PANI was obtained by varying the concentration PANI in NMP. The electrodes were dried overnight at 100 °C. For making the liquid-state device, two electrodes as prepared above were separated using a polypropylelene membrane as a separator and was tested by dipping in 0.5 M H_2SO_4. To make the solid-state supercapacitors, the PVA-H_2SO_4 aqueous solution was used as the electrolyte. This was coated onto both surfaces of the PANI coated carbon paper electrode using a K-control coater and thereafter the paper was dried using an air gun. This facilitates impregnation of PVA-H_2SO_4 gel-plasticized polymer matrix within the carbon matrix along the fibrous surface which was initially covered by PANI. Two such electrodes were taken after ensuring that a fine layer of PVA-H_2SO_4 is formed on one side to serve as an effective separator as well. Two pieces were attached together by applying pressure. The film formed in between the electrodes will prevent the short circuit by acting as a separator.

Characterization. Structure and morphology of the materials and device were analyzed using a Quanta Scanning Electron Microscope. All the electrochemical studies were carried in a Bio-Logic SP-300 Potentio-Galvanostat. The required electrical contacts from the electrodes were made by using metal crocodile clips. The cyclic voltammetry measurements were taken at different scan rates from 10 to 150 mV/s by maintaining a potential window of 0.8 V. The charge−discharge measurement was done at different current densities (0.5 to 20 A/g) in the potential range of 0−0.8 V. Cycling stability was done by chrono charge−discharge method at 5 A/g current density. Electrochemical impedance (EIS) analysis was carried out from 106 to 0.01 Hz frequency against the open circuit potential with a sine amplitude of 10 mV (V_{rms} = 7.07 mV). The EIS data was analyzed using the EC-Lab Software V10.19. For an effective comparison, the experiments were conducted in a plain current collector by using a Grafoil paper and by taking both liquid and solid electrolytes. Leakage current from the plot of current vs time was obtained by charging the cell using a low current density up to 0.8 V and keeping the cell at 0.8 V by the chrono-amperometric technique. Voltage drop of the cell was measured for 24 h by charging the cell at 0.8 V for 20 min followed by measuring the open circuit potential. Four all-solid-state supercapacitors (ASSPs) having 1.5 mg/cm^2 loading on each electrode were connected in series to get a working potential of 3 V for glowing a LED.

3. RESULTS AND DISCUSSION

Doped PANI was synthesized by chemical oxidation of aniline using ammonium persulfate in acidic condition.[25] The solvent selected here was *N*-methyl-2-pyrrolidone (NMP),[30] and the concentration was carefully adjusted to get the proper distribution of PANI particles on to the carbon fibers without blocking the pores. This was essential for attaining enough space for the penetration of the solid electrolyte. PANI solution was manually coated onto the porous carbon paper using a steel rod over a smaller area, while coating on larger areas was performed by an automated K-coater. For incorporating the solid-electrolyte in the solid-state device, an aqueous solution of PVA-H_2SO_4 was applied on to the PANI coated porous carbon paper. The density of PVA was tuned for easy penetration of the solid electrolyte into the pores of the PANI coated carbon paper. Two such electrodes are sandwiched together to form the device. The device fabrication steps are shown schematically in Figure 1a. Optical images of a single cell device and 4-cells in series powering an LED are shown in Figure 1b and 1c, respectively.

Scanning electron microscopy (SEM) and elemental mapping of the surface of carbon paper using energy-dispersive X-ray spectroscopy (EDX) show a clear picture of the surface morphology of the device. The SEM images of the bare carbon paper in Figure 2a and in Supporting Information, Figure S1a-b

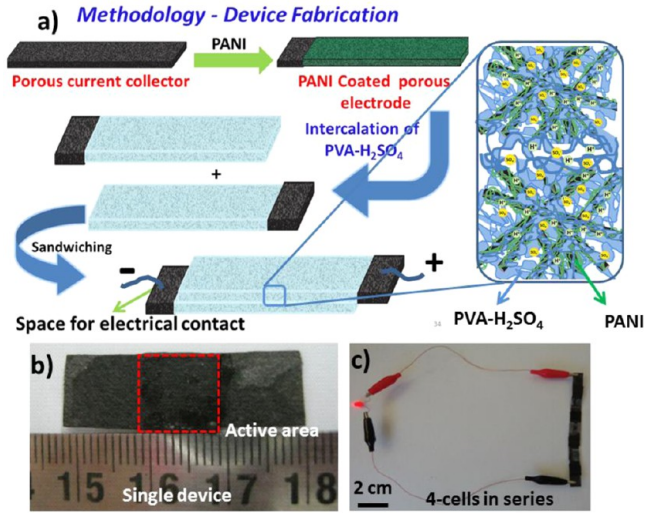

Figure 1. (a) Schematics of the ASSP representing the steps involving the coating of PANI onto the carbon paper, incorporation of PVA-H_2SO_4 into the porous PANI/carbon paper, and sandwiching of electrodes by applying pressure to make the all-solid-state-supercapacitor. (b) Optical images of 1 cm^2 prototype ASSP. (c) LED powered by a four-cell assembly connected in series.

show high porosity of the matrix which is formed by homogeneous alignment of uniform fibers having a diameter of ~5 μm. To validate the role of the porous matrix of the carbon paper, we used a Grafoil substrate as well, which is a plain nonporous conducting substrate, as a current collector. The corresponding SEM image of Grafoil is given in Supporting Information, Figure S1c. Figure 2b shows the SEM image of the carbon paper loaded with 1.5 mg/cm^2 PANI (for the images corresponding to the different loading of PANI as 0.3, 1.5, 3, and 5 mg/cm^2, refer to Supporting Information, Figure S1d-f). The particle size of PANI is small because of the higher solubility of PANI in NMP, which helps in attaining uniform coating along the individual fibers of the carbon paper throughout the matrix. However, at higher loading, more PANI particles are accumulated at the surface which in turn reduces the porosity and is evident from Supporting Information, Figure S1d-f. The carbon surface after the PVA-H_2SO_4 coating is shown in Figure 2c which reveals a well intercalated PVA-H_2SO_4 matrix.

Cross-sectional SEM images and elemental mapping along the cross-section of the device gives a clear picture of the expected high integrity and enhanced electrode−electrolyte interface within the system (Figure 3a−c). The total thickness of the device is only 0.80 mm which comprises a fine film of the gel electrolyte possessing a thickness of 0.12 mm in between the PANI coated carbon paper. The EDX elemental mapping shows the intercalated PANI particles and PVA-H_2SO_4 inside the carbon fiber matrix. The nitrogen (N) mapping in Supporting Information, Figure S2a corresponds to the cross-section of the device possessing a catalyst loading of 0.30 mg/cm^2, which clearly shows that PANI is uniformly distributed throughout the matrix and not restricted only at the surface. Similarly, sulfur (S) mapping at the same location as shown in Figure 3a indicates the presence of S into either side of the PVA-H_2SO_4 film. This unambiguously confirms the diffusion of PVA-H_2SO_4 through the carbon fibers, which leads to an intimate electrode−electrolyte interface in the system. Further, the diffusive nature of the solid-electrolyte appeared to be decreasing with higher loading of PANI, which is clear from the cross-sectional mapping of the corresponding devices which are having different PANI loading as shown in Figure 3b and c. The gradual change in the porosity of the carbon paper with the loading of PANI is clear from Supporting Information, Figure S1d-f. It is clear from these sets of figures that higher loading of PANI leads to filling of the pores heavily so that the space available for the intercalation of the polymer electrolyte is decreasing. The SEM cross-section images and elemental mapping also emphasize the need for special attention to be taken with higher loading of PANI to establish adequate integrity. Such benefits in establishing extended electrode−electrolyte interfaces will help to achieve very high areal capacitance without compromising the specific capacitance. This extended and well-distributed interfacial structure nearly mimics an interfacial structure which can be expected in a system based on the conventional liquid electrolytes.

Electrochemical charge storage properties of the PANI coated electrodes were analyzed initially in acidic medium containing 0.5 M H_2SO_4 and subsequently the tests were done using the systems based on the gel electrolyte. In the case of the tests in 0.5 M H_2SO_4, the two PANI coated electrodes were separated by a polycarbonate film, and the assembly was dipped in the electrolyte. Cyclic voltammograms (CVs) and charge−discharge measurements were recorded by varying the scan rates and current densities from 10 to 150 mV/s and 0.5 to 20 A/g, respectively. Since we used symmetrical two electrodes for the testing, capacitance values calculated from the CV and charge−discharge profiles were multiplied by a factor of 2 to obtain the capacitance of the single electrode (Supporting Information, eqs 1 and 2). As mentioned before, we have prepared nonporous electrodes by coating PANI on Grafoil along with the PANI coated porous carbon electrodes. Grafoil with a PANI loading of 1.5 mg/cm^2 displays a capacitance of 300 F/g when the CV was recorded at a voltage scan rate of 10

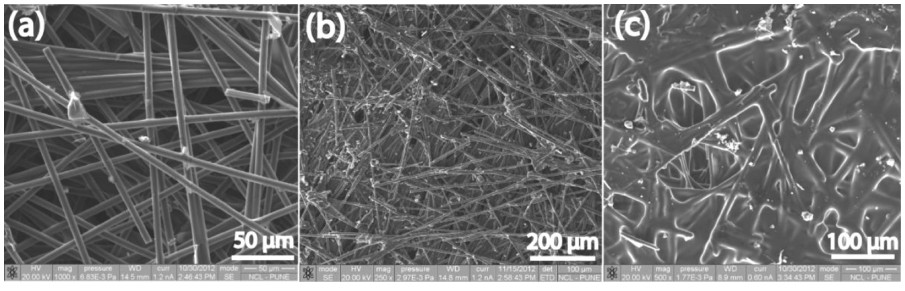

Figure 2. SEM images of (a) porous carbon paper, (b) PANI (1.5 mg/cm^2) coated carbon paper, and (c) intercalated gel-electrolyte inside the PANI/carbon paper.

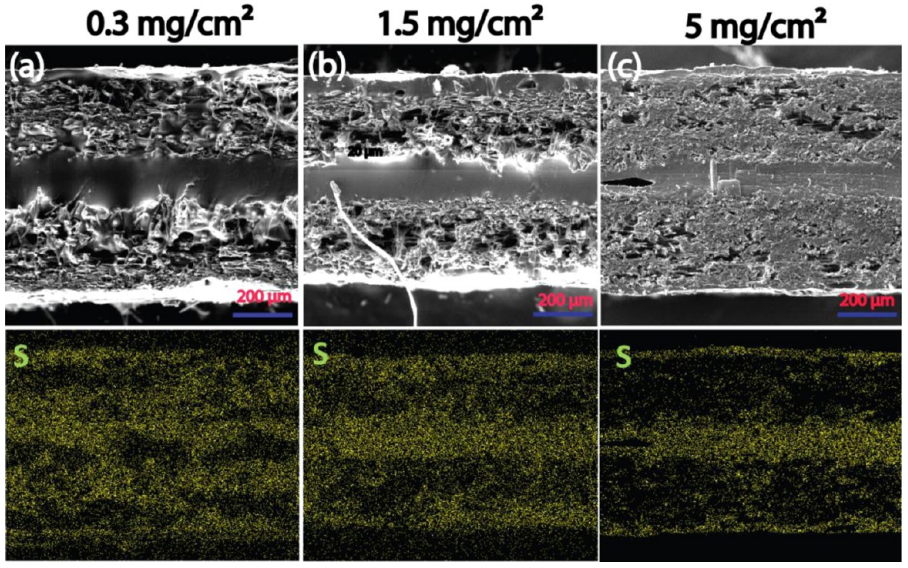

Figure 3. Cross-sectional SEM images and the corresponding S-elemental mapping of the ASSP with different loading of PANI: (a) 0.3 mg/cm^2, (b) 1.5 mg/cm^2, and (c) 5.0 mg/cm^2.

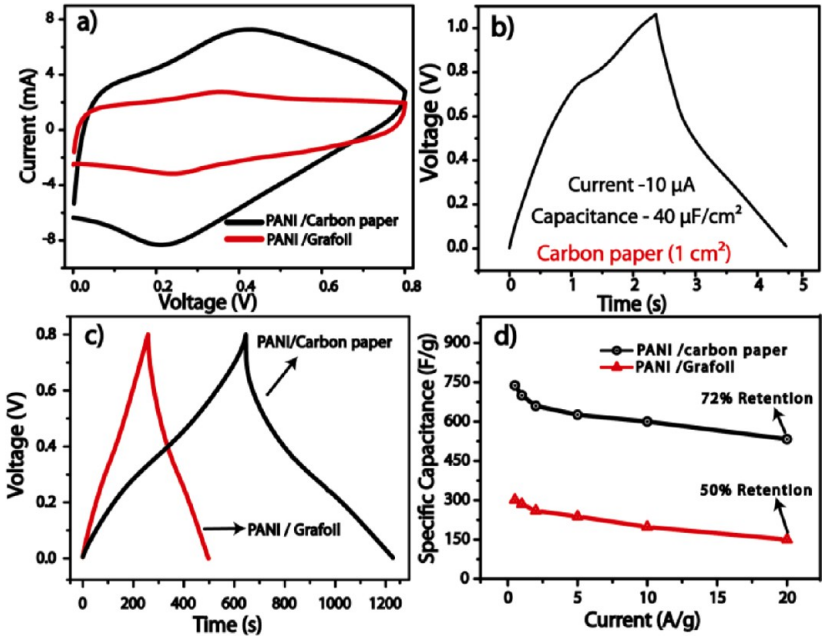

Figure 4. Comparison of (a) CVs at a scan rate of 10 mV/s for the systems made by using porous carbon and Grafoil as the substrates, (b) charge−discharge curve of blank carbon paper at a current density of 10 μA, (c) charge−discharge profiles at a current density of 0.5 A/g of the PANI coated carbon paper and Grafoil, (d) the plots indicating the change in the specific capacitance with current density for the carbon paper and Grafoil based systems. All the experiments are done in 0.5 M H_2SO_4 in a 2-electrode assembly.

mV/s (Figure 4a). This value is in good agreement with the reported capacitance of PANI[29,31,32] prepared by the same synthetic procedure. Now, looking at the performance of the porous carbon paper based electrode possessing the same PANI loading, an interesting leap in capacitance of 2.3 fold, leading to a value of 693 F/g at 10 mV/s, has been achieved in 0.5 M H_2SO_4 as shown in Figure 4a. It should be noted that the contribution of the porous carbon paper toward the capacitance is only 40 μF/cm^2 (Figure 4b), and, hence, can be neglected while considering the overall capacitance. The charge−discharge method also displays similar results in which the PANI coated carbon paper gives a mass specific capacitance of 700 F/g and an areal capacitance of 1.05 F/cm^2. Contrary to this, the corresponding values with the Grafoil counterpart are only 300 F/g and 0.45 F/cm^2 respectively at 0.5 A/g current density (Figure 4c). The obtained specific capacitance of 700 F/g for PANI and an areal capacitance of 1.05 F/cm^2 are much higher than the corresponding reported capacitance values for pure PANI.[29,32−35] Apart from this, Figure 4d shows an excellent capacitance retention of 72% for the PANI coated carbon paper even at a fast discharging rate of 20 A/g compared a 50% retention of the PANI/Grafoil system (remaining plots are given in Supporting Information, Figure S3). Thus, the cyclic voltammetry and charge−discharge methods reveal a huge difference in the capacitance values when the substrate morphology changes from nonporous to

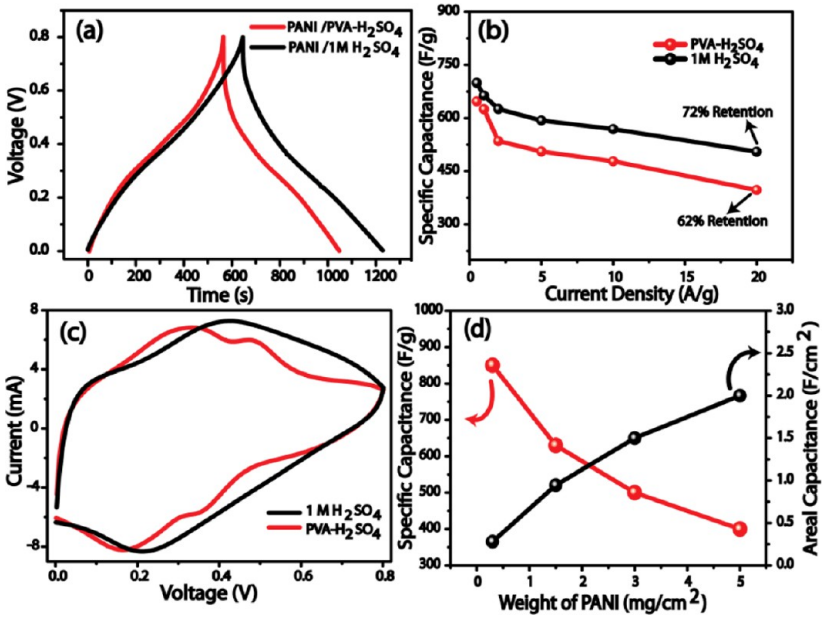

Figure 5. Comparison of (a) charge–discharge profiles at a current density of 0.5 A/g of the PANI coated carbon paper in 0.5 M H_2SO_4 and PVA-H_2SO_4, (b) plots indicating the change in the specific capacitance with current density for the solid and liquid-state systems, (c) CV for the solid and liquid-state systems taken at a scan rate of 10 mV/s, and (d) plots corresponding to the specific capacitance vs areal capacitance of the solid-state system.

Table 1. Comparative Performance of ASSP with a PANI Loading of 1.5 mg/cm^2 Compared to the Literature Reported Solid Devices

	solid electrolyte	specific capacitance (F/g)	areal capacitance (mF/cm^2)	internal resistance (Ω)	leakage current (μA)	energy density (W h/kg)	voltage window	ref
in this work	PVA-H_2SO_4	638	957	1 Ω/cm^2	15	14.36	0.8	
carbon nanoparticles/ MnO_2	PVA-H_3PO_4	675	20	4	15	4.8	0.8	22
hierarchical $GeSe_2$	PVA-H_2SO_4	300	0.25	30	0.02	2.6[a]	0.5	18
N,B doped 3D graphene	PVA-H_2SO_4	62				8.7	1	39
SWCNT	PVA-H_3PO_4	35	1000	60		6	1	
CNT-PANI	PVA-H_2SO_4	350	800	11	17	7.1	0.8	20
nanoporous Gold-PPy	PVA-$HClO_4$	250	1.8			6.7	0.8	36
PANI/Au paper	PVA-H_3PO_4		50	25	10	0.01 W h/cm^3	0.8	35

[a]Calculated.

porous even though both are having the same PANI content. This difference can be clearly attributed to the utilization of high porosity carbon paper for achieving enhanced electrode–electrolyte interface for PANI upon its coating on the surface.

Fabrication of the ASSP requires replacement of the liquid electrolyte with the solid electrolyte. The above results using the liquid electrolyte clearly indicate the superiority of the porous substrate as the current collector to establish higher area of the electroactive material. Once this condition is maintained, a proper intercalation by a solid electrolyte which gives a closely matching interfacial structure with the electrode material is expected to narrow down the differences in the performances between the solid and liquid systems. To conceive this condition, the solid electrolyte, which will mimic the nature of the liquid electrolyte, should lead to very high interfacial area inside the porous current collector. We have overcome this issue by using PVA-H_2SO_4 gel polymer electrolyte by in situ solidifying inside the porous current collector which is already coated with PANI, but still bearing enough porosity to accommodate the gel electrolyte. Since the porosity is still sufficient inside the PANI/carbon paper for making the intercalated electrode-gel electrolyte interface, the system more or less mimics an interfacial structure similar to a case where a liquid electrolyte is used.

This strategy has been realized successfully as reflected from the measured capacitance of the ASSP (active material is 1.5 mg/cm^2), which shows a capacitance of 647 F/g at a current density of 0.5 A/g by the galvanostatic charge–discharge method (Figure 5a). The retention of capacitance of the ASSP with the current density as shown in Figure 5b shows that the ASSP could retain 400 F/g even at a high current density of 20 A/g. The capacitance value obtained by the cyclic voltametry is 568 F/g at 10 mV/s compared to 700 F/g measured by using the liquid electrolyte (Figure 5c). The CV profiles of the solid and liquid based systems have similar features even though at higher potentials, the solid-state system shows lower current. The CV profiles of the ASSP at different scan rates and the specific capacitance at each scan rate compared to the liquid state are given in Supporting Information, Figure S4a-b. In both the cases, closely comparable capacitance retention has been

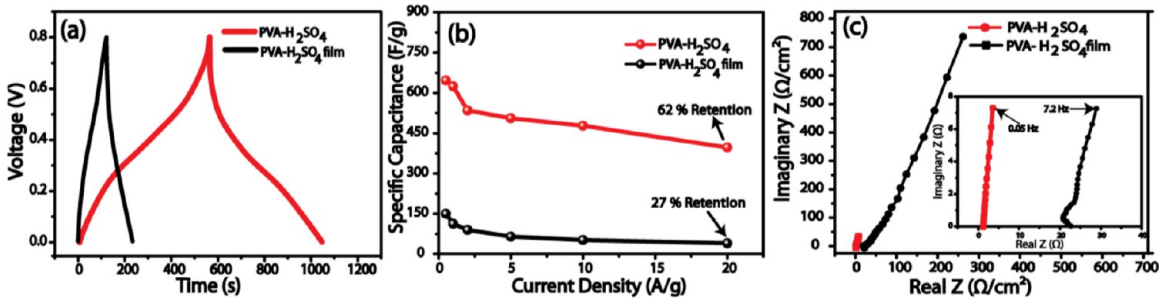

Figure 6. Performance characteristics of the solid-state devices formed by the present approach and the one made by using a polymer film as in the case of the conventional systems: (a) comparison of the charge−discharge profiles measured at 0.5 A/g current density, (b) comparison of the change in specific capacitance with varied current. (c) Nyquist plot of the ASSP using PVA-H_2SO_4 in the present strategy and conventional solid film method with enlarged part of the high frequency region in the inset.

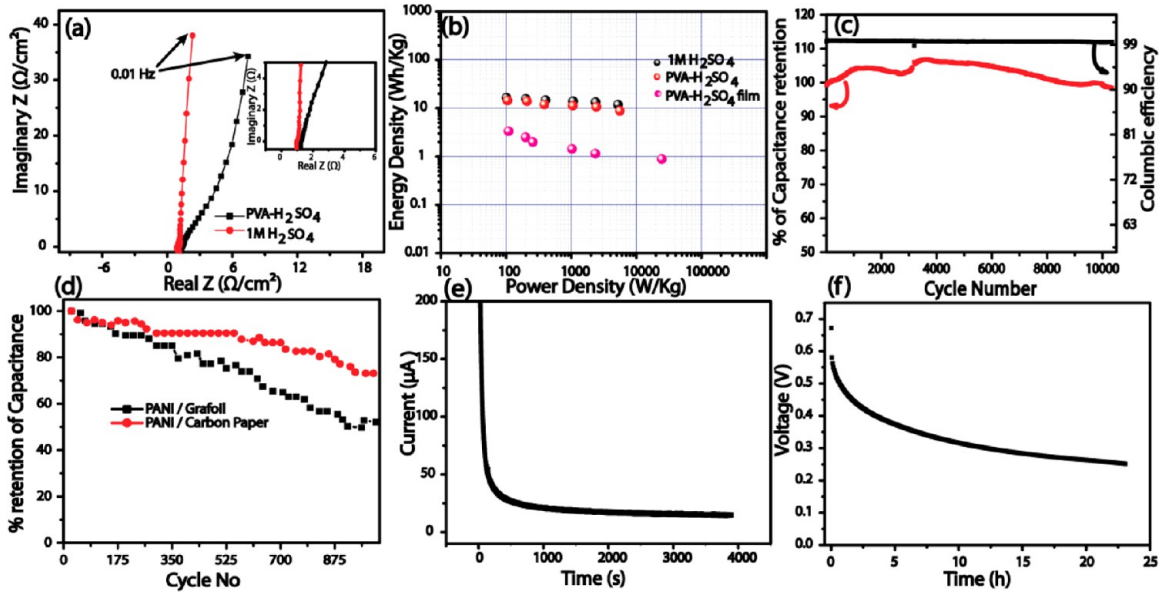

Figure 7. (a) Comparison of the Nyquist plots of the ASSP using PVA-H_2SO_4 as the electrolyte with the corresponding liquid-state system made by using 0.5 M H_2SO_4. (b) Ragone plots created by calculating the energy density and power density from the charge−discharge method; (c) cycle stability test extending for a period of 10000 cycles of the ASSP carried at a current density of 5 A/g; (d) comparative cycle stability done at a charge−discharge current density of 5 A/g in 0.5 M H_2SO_4 for Grafoil and carbon paper each having a PANI loading of 1.5 mg/cm^2. Panels (e) and (f) represent the leakage current measured by keeping the device at 0.8 V and potential drop with respect to time measured after raising the potential to 0.8 V of ASSP.

observed with respect to the variation of the voltage scan rate from low to high (Supporting Information, Figure S4b). The capacitance value of the ASSP is almost 93% of the capacitance obtained for the liquid state system using 0.5 M H_2SO_4 by the charge−discharge method. Charge−discharge profile and the variation of the specific capacitance with change in current density are given in Supporting Information, Figure S4c-e for the different PANI loaded samples. The areal capacitance is estimated to be 1 F/cm^2 for PANI with its loading of 1.5 mg/cm^2.

Variation of specific capacitance vs areal capacitance is given in Figure 5d which is calculated from the charge−discharge method. To the best of our knowledge, the specific and areal capacitances obtained in the present case are the highest ever reported for the ASSPs. A comparative literature survey has been given in Table 1. Even at a very high areal capacitance of 2 F/cm^2, the device shows a specific capacitance of 400 F/g. It should be noted that many of the ASSPs reported have very low areal capacitances in microfarads even though they have high specific capacitance[22,35,36](Table.1).The specific capacitance could reach up to 850 F/g with a low PANI loading of 0.3 mg/cm^2, where the areal capacitance is 0.28 F/cm^2. These variations are expected and are in accordance with the aforementioned results of the SEM and elemental mapping of the cross-section of the devices possessing varying loading of PANI. As the PANI content increases, the pores are getting filled and subsequently most of the PANI particles stay at the surface and prevent penetration of PVA-H_2SO_4 into the carbon paper. This leads to a lower electrode−electrolyte interface, which is clear from the comparative S elemental mapping in Figure 3a−c.

For comparing the design of the electrode−electrolyte interface with the conventional approach involving an ion conducting membrane as a separator between the electrodes, we fabricated a system by sandwiching a PVA-H_2SO_4 film in between the PANI coated carbon papers by hot pressing. Because of the lower electrode−electrolyte contact, the system gives a significantly low specific capacitance of 150 F/g at 0.5 A/g and a PANI loading of 1.5 mg/cm^2 (Figure 6 a−b) compared to 647 F/g as obtained in the previous case by

applying the gel-electrolyte directly on the electrodes. Apart from the lower specific capacitance, the device also shows very low capacitance retention (27% when the current directly increased to 20 A/g from 0.5 A/g). The high internal resistance of 20 Ω/cm^2 (Figure 6) measured from the x-intersect of the Nyquist plot of impedance analysis validates the reason for the poor capacitance retention of the system. This clearly shows the advantages of our design to enhance the electrode−electrolyte interface rather than having a solid film between the electrodes.

Impedance analysis of the ASSP confirms the high charge storage properties obtained by both cyclic voltammetry and chrono charge−discharge methods. The high retention of capacitance under fast charge−discharge conditions is possible only if the system assists very fast ion diffusion in response to the large perturbation. Two factors which have the key role here are the ESR and the charge-transfer resistance. Estimated ESR from the Nyquist plot of the device is only 1 Ω/cm^2 (Figure 7a). The liquid and solid systems have only 0.1 Ω differences, which explain the superior power rate and high retention of the ASSP. It is also interesting to note that the ESR of the solid device made by using the PVA-H_2SO_4 film shows a huge ESR of 20 Ω/cm^2 (Figure 6c). Further, in our ASSP, we could not resolve the characteristic high frequency semicircle even in the zoomed image in Figure 7a, confirming that there is very less charge-transfer resistance in the system.

Energy density and power density are calculated from the charge−discharge method after excluding the weight of the carbon paper and electrolyte. The corresponding Ragone plot is shown in Figure 7b. The PANI in the solid device shows an energy density of 14.3 Wh/kg at a power density of 105 W/kg compared to 3.3 W h/kg of the device which uses a polymer film. The energy density obtained here is probably the highest among the other reported values of ASSPs (Table 1). At a higher power rate of 5.6 kW/kg, the ASSP based on the current approach could keep an energy density of 8.8 W h/kg whereas the film based system shows an energy density of only 1.1 W h/kg at a power rate of 2.3 kW/kg. The volumetric energy density of the whole device including the carbon paper and the solid electrolyte is 0.53 mWh/cm^3.

Extended cycling stability is an essential criterion for any charge storage devices. It is found that the architecture improves the stability along with the capacitance. We carried out 10000 continuous cycling at a current density of 5 A/g of ASSP which was showing a capacitance of 638 F/g. Percentage capacitance retention and coulombic efficiency during the 10000 cycles are plotted in Figure 7c. Excellent stability was obtained during the cycling with less than 2% degradation and nearly 100% coulombic efficiency during the entire cycling. In contrast to the low stability of PANI in liquid electrolyte (Figure 7d), the enhanced stability of PANI in ASSP is clearly explained by the role of PVA as the binder. Apart from the role as the electrolyte matrix in the device, PVA also plays an integral role by providing a means to hold the PANI moiety tightly. On the other hand, in the liquid electrolyte, the relative movement of the electrolyte will enhance the detachment of the electrode material from the electrode as we have not applied any extra binder for ensuring mechanical stability. The obtained cycle stability of the solid supercapacitors is much superior to those in the literature reports.[20,29,37]

The prototype device made here is a significantly lightweight assembly because of the low density of the carbon paper. The whole device has a weight of only 110 mg (Supporting Information, Figure S5d) including the space given for the contact, which is inactive in terms of charge storage. The whole device including the electrolyte shows a capacitance of 12.5 F/g, which is double as compared to the commercially available supercapacitors with liquid electrolytes.[38] It should be noted that the amount of the polymer electrolyte can still be reduced as we have given extra thickness (120 μm) between the electrodes. This will further decrease the whole device weight. The whole device dimension is also very promising as the thickness is only 0.8 mm. Leakage current and self-discharge values are two essential parameters of supercapacitors in terms of the practical usage. We measured the leakage current of the device by charging at 0.8 V and by monitoring the current required to maintain that potential. Normally, the leakage current of the supercapacitors is higher than that in the Li-ion batteries. Here, the device leakage current is only 50 μA at 200 s, which reached to 16 μA at 2000 s (Figure 7e). This value is less compared with the values reported in the literature.[20] The device could hold 0.25 V even at 24 h which is also comparable to the literature values[22] (Figure 7f). Further, we connected four such devices in series to make an LED glow whose minimum working potential was 2 V as shown in Figure 1c. The LED could be made to glow more than 1 min, and the intensity of its illumination diminishes when the potential reaches to 2 V (see Supporting Information video). The CV at 10 mV/s and the charge−discharge profile at 10 mA of the above coupled device are shown in Supporting Information, Figure S6a−-b.

4. CONCLUSION

In conclusion, we have reported a high performance ASSP made by intercalating a gel-polymer electrolyte, that is, PVA-H_2SO_4, with PANI-coated carbon paper, which in turn enhances the electrode−electrolyte interface of the resulting device. The gel electrolyte also simultaneously serves as the separator between the electrodes when the electrodes are combined together to form a cell. Cross-sectional elemental mapping and SEM images display the proof of concept. The enhanced interface helps the solid device to perform like a liquid counterpart showing a specific capacitance of 647 F/g for PANI with an areal capacitance of 1 F/cm^2 at 0.5 A/g. It shows a retention of 62% of its capacitance at a current density of 20 A/g. High integrity of the electrode−electrolyte phases helps the device to attain a very low ESR of 1 Ω/cm^2. The device shows excellent cycle stability and coulombic efficiency. This approach could significantly narrow down the difference between the charge storage properties of the solid- and liquid-state supercapacitor devices. The strategy conceived here is not restricted only to PANI, but can also be further applied to different charge storage materials in conjunction with highly porous and conducting substrates. Thus, the evolved concept has the potential to make significant advancements in the energy storage technologies by providing efficient lighter, thinner, safer, and cheaper electric devices.

■ ASSOCIATED CONTENT

Supporting Information

Calculation of capacitance, energy density, power density, and conductivity. SEM images of Carbon paper, Grafoil, and PANI/coated carbon paper. Cross sectional Nitrogen mapping of the ASSPs. Detailed CV and charge discharge curves of various samples. CV and charge discharge curve of four ASSPs connected in series. Video (.avi format) showing ASSPs

powered LED glow. This material is available free of charge via the Internet at http://pubs.acs.org.

AUTHOR INFORMATION

Corresponding Author

*E-mail: k.sreekumar@ncl.res.in.

Notes

The authors declare no competing financial interest.

ACKNOWLEDGMENTS

Special thanks go to Dr. S. Pal, Director, NCL, Pune, for his continuous encouragement. B.A. and K.S. acknowledge CSIR and DST (Project No. SR/S1/PC-05/2011), respectively for the financial assistance

ABBREVIATIONS

ASSP, All-solid-state-supercapacitor; PANI, Polyaniline

REFERENCES

(1) Yang, Z.; Zhang, J.; Kintner-Meyer, M.; Lu, X.; Choi, D.; Lemmon, J.; Liu, J. *Chem. Rev.* **2011**, *111*, 3577−3613.
(2) Palacin, M. R. *Chem. Soc. Rev.* **2009**, *38*, 2565−2575.
(3) Choi, N. S.; Chen, Z.; Freunberger, S. A.; Ji, X.; Sun, Y. K.; Amine, K.; Yushin, G.; Nazar, L. F.; Cho, J.; Bruce, P. G. *Angew. Chem., Int. Ed.* **2012**, *51*, 9994−10024.
(4) Conway, B. E. *Electrochemical Supercapacitors: Scientific Fundamentals and Technological Applications*; Plenum Press: New York, 1999; p 1.
(5) Winter, M.; Brodd, R. J. *Chem. Rev.* **2004**, *104*, 4245−4270.
(6) Simon, P.; Gogotsi, Y. *Nat. Mater.* **2008**, *7*, 845−854.
(7) Arbizzani, C.; Mastragostino, M.; Soavi, F. *J. Power Sources* **2001**, *100*, 164−170.
(8) Zhang, Y.; Feng, H.; Wu, X.; Wang, L.; Zhang, A.; Xia, T.; Dong, H.; Li, X.; Zhang, L. *Int. J. Hydrogen Energy* **2009**, *34*, 4889−4899.
(9) Vellacheri, R.; Pillai, V.; Kurungot, S. *Nanoscale* **2012**, *4*, 890−896.
(10) Catia, A.; Maurizio, B.; Dario, C.; Mariachiara, L.; Francesca, S.; Marina, M. *J. Power Sources* **2008**, *185*, 1575−1579.
(11) Wright, P. V. *Electrochim. Acta* **1998**, *43*, 1137−1143.
(12) Song, J. Y.; Wang, Y. Y.; Wan, C. C. *J. Power Sources* **1999**, *77*, 183−197.
(13) Agrawal, R. C.; Pandey, G. P. *J. Phys. D: Appl. Phys.* **2008**, *41*, 223001.
(14) Kyung-Won, P.; Hyo-Jin, A.; Yung-Eun, S. *J. Power Sources* **2002**, *109*, 500−506.
(15) Lewandowski, A.; Zajder, M.; Frackowiak, E.; Béguin, F. *Electrochim. Acta* **2001**, *46*, 2777.
(16) White, A. M.; Slade, R. C. T. *Synth. Met.* **2003**, *139*, 123.
(17) Dhanraj, R.; Meenu, V.; Nazrul, I.; Ramaiyan, K.; Ulhas, K.; Sreekumar, K.; Vijayamohanan, P. *J. Appl. Electrochem.* **2009**, *39*, 1097−1103.
(18) Wang, X.; Liu, B.; Wang, Q.; Song, W.; Hou, X.; Chen, D.; Cheng, Y.-B.; Shen, G. *Adv. Mater.* **2013**, *25*, 1479.
(19) Kaempgen, M.; Chan, C. K.; Ma, J.; Cui, Y.; Gruner, G. *Nano Lett.* **2009**, *9*, 1872−1876.
(20) Meng, C.; Liu, C.; Chen, L.; Hu, C.; Fan, S. *Nano Lett.* **2010**, *10*, 4025−4031.
(21) Yuan, L.; Xiao, X.; Ding, T.; Zhong, J.; Zhang, X.; Shen, Y.; Hu, B.; Huang, Y.; Zhou, J.; Wang, Z. *Angew. Chem., Int. Ed.* **2012**, *51*, 4934−4938.
(22) Yuan, L.; Lu, X.-H.; Xiao, X.; Zhai, T.; Dai, J.; Zhang, F.; Hu, B.; Wang, X.; Gong, L.; Chen, J.; Hu, C.; Tong, Y.; Zhou, J.; Wang, Z. *ACS Nano* **2012**, *6*, 656−661.
(23) Mehta, V.; Cooper, J. *J. Power Sources* **2003**, 32−53.
(24) Haijun, Y.; Jihuai, W.; Leqing, F.; Youzhen, L.; Kaiqing, X.; Ziying, T.; Cunxi, C.; Shen, T.; Jianming, L.; Miaoliang, H.; Zhang, L. *J. Power Sources* **2012**, *198*, 402−407.
(25) MacDiarmid, A. G.; Epstein, A. J. *J. Chem. Soc., Faraday Trans.* **1989**, *88*, 317.
(26) Peng, C.; Hu, D.; Chen, G. Z. *Chem. Commun.* **2011**, *47*, 4105−4107.
(27) Li, H.; Wang, J.; Chu, Q.; Wang, Z.; Zhang, F.; Wang, S. *J. Power Sources* **2009**, *190*, 578−586.
(28) Snook, G. A.; Kao, P.; Best, A. S. *J. Power Sources* **2011**, *196*, 1−12.
(29) Wu, Q.; Xu, Y.; Yao, Z.; Liu, A.; Shi, G. *ACS Nano* **2010**, *4*, 1963−1970.
(30) Jain, R.; Gregory, R. *Synth. Met.* **1995**, *74*, 263−266.
(31) Ghosh, D.; Giri, S.; Mandal, A.; Das, C. K. *RSC Adv.* **2013**, *3*, 11676−11685.
(32) Zhang, H.; Wang, J.; Chen, Y.; Wang, Z.; Wang, S. *Electrochim. Acta* **2013**, *105*, 69−74.
(33) Liu, J.; Zhou, M.; Fan, L.-Z.; Li, P.; Qu, X. *Electrochim. Acta* **2010**, *55*, 5819−5822.
(34) Jyongsik, J.; Joonwon, B.; Moonjung, C.; Seong-Ho, Y. *Carbon* **2005**, *43*, 2730−2736.
(35) Yuan, L.; Xiao, X.; Ding, T.; Zhong, J.; Zhang, X.; Shen, Y.; Hu, B.; Huang, Y.; Zhou, J.; Wang, Z. *Angew. Chem., Int. Ed.* **2012**, *51*, 4934−4938.
(36) Meng, F.; Ding, Y. *Adv. Mater.* **2011**, *23*, 4098−4102.
(37) Ying-Ying, H.; Yi-Chen, L.; Yu-Kuei, H.; Chia-Chun, C.; Li-Chyong, C.; Kuei-Hsien, C. *J. Power Sources* **2010**, *195*, 4418.
(38) Chu, A.; Braatz, P. *J. Power Sources* **2002**, *112*, 236−246.
(39) Wu, Z.-S.; Winter, A.; Chen, L.; Sun, Y.; Turchanin, A.; Feng, X.; Müllen, K. *Adv. Mater.* **2012**, *24*, 5130−5135.